DATA-DRIVEN MODELLING OF THE INOSITOL TRISPHOSPHATE RECEPTOR (IP_3R) AND ITS ROLE IN CALCIUM INDUCED CALCIUM RELEASE (CICR)

IVO SIEKMANN[1], PENGXING CAO[2],
JAMES SNEYD[3] & EDMUND J. CRAMPIN[1,2,4]

[1] SYSTEMS BIOLOGY LABORATORY, MELBOURNE SCHOOL OF ENGINEERING, UNIVERSITY OF MELBOURNE, AUSTRALIA
[2] DEPARTMENT OF MATHEMATICS AND STATISTICS, UNIVERSITY OF MELBOURNE, AUSTRALIA
[3] DEPARTMENT OF MATHEMATICS, UNIVERSITY OF AUCKLAND, NEW ZEALAND
[4] SCHOOL OF MEDICINE, UNIVERSITY OF MELBOURNE, AUSTRALIA

1. INTRODUCTION

A number of models have been published that relate different physiological processes involving glial cells to calcium dynamics. De Pittà et al. [22] give an overview of current problems in the modelling of astrocytes. One area of continuing interest is the propagation of signals between astrocytes via intercellular calcium waves. Höfer et al. [42] investigated the spreading of signals between astrocytes via calcium waves based on a model by Sneyd et al. [76]. Bennett et al. [8, 7] developed a more detailed model of calcium waves that combines underlying calcium dynamics with ATP release by purinergic receptors in order to demonstrate that calcium waves depend on ATP release rather than on IP_3 diffusion through gap junctions as in the model by Höfer et al. [42]. Edwards and Gibson [27] later published a model that included both modes of signal propagation and concluded that both were necessary to account for data collected from the retina. Recently, the study of calcium waves has been extended from one- or two-dimensional to three-dimensional spatial domains [45]. Macdonald and Silva [50] model wave propagation on an astrocyte network derived from experimental data. The Bennett et al. model was used for investigating spreading depression, a wave of electrical silence that propagates through the cortex and depolarises neurons and glial cells [9].

A fundamental problem in calcium dynamics in general is the question how multiple signals can be encoded by the dynamics of a single quantity, the concentration of calcium. De Pittà et al. [24, 20, 23] investigated how a stimulus could be encoded via the frequency or the amplitude or both frequency and amplitude which demonstrates that two different signals can be represented independently in an individual calcium signal. Dupont et al. [26] showed in a detailed model how the signal received by a particular glutamate receptor is encoded via calcium oscillations.

Lavrentovich and Hemkin [46], Zeng et al. [87], Riera et al. [62, 63] investigated spontaneous calcium oscillations in astrocytes and Li et al. [47] explored their role in spreading depression.

Also the coupling of astrocyte network with the neural network has been investigated. At the single-cell level, De Pittà et al. [21] modelled the interaction of an astrocyte with a synapse. Allegrini et al. [1], Postnov et al. [59] study the influence of a network of astrocytes on a neural network.

Most recently, Barrack et al. [5, 6] explored the role of calcium signalling in neural development. By coupling calcium dynamics with a model of the cell cycle they examine how glial progenitors differentiate to neurons triggered by a calcium signal.

This review of the modelling literature on glial cells clearly demonstrates that the importance of calcium dynamics is well recognised—the majority of studies in the literature accounts for calcium signalling and often models are used to find a link of physiological processes with

calcium signalling. In many cell types including glial cells the inositol trisphosphate receptor (IP_3R) plays a crucial role in inducing oscillatory Ca^{2+} signals. In the presence of IP_3, opening of IP_3R channels leads to Ca^{2+} release from the endoplasmic reticulum (ER), an intracellular compartment with a very high Ca^{2+} concentration a few orders of magnitude higher than that of the cytoplasm. The IP_3R is activated by Ca^{2+} so that such a release event dramatically increases the open probability of the IP_3R which induces further release of Ca^{2+}(henceforth called calcium-induced-calcium-release, or CICR) until a high Ca^{2+} concentration in the channel environment eventually inhibits the IP_3R.

The Li-Rinzel model [48], an approximation of the classical De Young-Keizer model [25], is by far the most commonly used representation of the IP_3R in models of glial cells. Only Allegrini et al. [1] and Lavrentovich and Hemkin [46] chose different models based on Atri et al. [3] or Tu et al. [82], respectively. Dupont et al. [26] use the model by Swillens et al. [79] that explicitly accounts for the effect of interactions in a cluster of IP_3R channels. Early models of the IP_3R were designed to account for the bell-shaped Ca^{2+} dependency of the open probability p_O of the channel described by Bezprozvanny et al. [10]. Since then the dynamics of IP_3R in response to varying concentrations of IP_3, Ca^{2+} and ATP has been characterised much more comprehensively as well as the differences between the different isoforms of the IP_3R (among the models mentioned above, in fact, only Tu et al. [82] accounts for the fact that astrocytes predominantly express type II IP_3R).

The scope of current data-driven models of ion channels has advanced beyond representing the average open probability p_O. Recent models capture the stochastic opening or closing of single IP_3Rs in aggregated Markov models i.e. instead of only modelling the stationary behaviour of the channel they represent the dynamics of the IP_3R (Section 3.4). Accurate representation of IP_3R dynamics depends on various sources of experimental data (Sections 3.1-3.2) as well as appropriate statistical methods for fitting Markov models to these data (Section 3.5). Statistical methods automate the process of estimating parameters for a given Markov model. Thus, the main challenge of data-driven ion channel modelling is to define the structure of a Markov model which allows the integration of various sources of experimental data. We illustrate this process with two recent examples of models for the IP_3R (Sections 3.6 and 3.7).

Once a model for a single channel has been developed, data from small clusters of channels can be used to determine how well the behaviour of a cluster is represented by an ensemble of single-channel models (Section 4.1). Studying the influence of an IP_3R model on calcium dynamics allows us to evaluate the relative importance of different aspects of single-channel dynamics. Cao et al. [14] showed that the essential features of calcium dynamics in airway smooth muscle could be preserved after iteratively simplifying the IP_3R model by Siekmann et al. [73] to a two-state model that only accounted for the switching between the inactive "park" and the active "drive" mode. In Section 4.2 it is shown that this also applies to the puff distribution. This demonstrates that modal gating is the most important regulatory mechanism of the IP_3R. It also emphasises that data-driven modelling of ion channels does not necessarily have to lead to detailed models based on complicated model structures but rather can be used so that relevant data is selected to represent ion channels at the appropriate level of complexity for a given application.

2. Mathematical models of calcium dynamics/CICR

The purpose of a mathematical model of CICR is to explain the emergence of complex intracellular calcium dynamics such as oscillations as the result of interdependent calcium fluxes. This comprises both fluxes into and out of the cell as well as the exchange between the cytosol and intracellular stores (Figure 1).

The dynamics of cytosolic (c) and stored calcium (c_{ER}) resulting from these fluxes can be represented by a system of differential equations:

$$\frac{dc}{dt} = J_{IP_3R} + J_{RyR} + J_{in} - J_{pm} - J_{SERCA} \tag{1}$$

$$\frac{dc_{ER}}{dt} = \gamma(J_{SERCA} - J_{IP_3R} - J_{RyR}) \tag{2}$$

Here, J_{in} is calcium influx from the extracellular space via calcium channels located in the cell membrane, J_{pm} accounts for calcium removed from the cell by the plasma membrane pump. J_{IP_3R} and J_{RyR} represent calcium release from the endoplasmic reticulum (ER) through the IP_3R and the RyR, respectively, and J_{SERCA} stands for reuptake of calcium into the ER by the SERCA pump. The conversion factor γ, the ratio of the cytoplasmic volume to the ER volume, is necessary because calcium concentrations are calculated with respect to the different volumes of these two compartments. The model (1), (2) provides a description of Ca^{2+} concentrations across the whole cell. This means that we cannot account for spatial effects due to heterogeneities of the spatial distribution of IP_3R, SERCA and other relevant components of the system. By using a deterministic model we further assume that the various Ca^{2+} fluxes can be described as deterministic after averaging over a large number of channels and transporters. In Section 4 we will consider a stochastic model over a small spatial domain for a cluster of interacting IP_3Rs.

In a whole-cell model of calcium dynamics such as (1), (2), a representation of the IP_3R must, in principle, just provide a functional expression for

$$J_{IP_3R}([IP_3], [Ca^{2+}], [ATP]), \tag{3}$$

the ligand-dependent flux through IP_3R channels present in a cell. Because the calcium concentration $[Ca^{2+}]$ is time-dependent, J_{IP_3R} varies over time. In the early days of modelling of the IP_3R, phenomenological models were used for representing the IP_3R flux. A good example is the model by Atri et al. [3]:

$$J_{IP_3R}(p, c) = N_{open} k \left(\mu_0 + \frac{\mu_1}{k_\mu + p}\right)\left(b + \frac{V_1 c}{k_1 + c}\right) \tag{4}$$

where $p = [IP_3]$, $c = [Ca^{2+}]$ and N_{open} is the number of open channels. The model by De Young and Keizer [25] is derived from more detailed assumptions on chemical interactions of the channel with its ligands. In Section 3.6 we present a more recent model [84] that is representative for this approach. The Hill function-type terms in (4) enabled Atri et al. to interpret their model in terms of a physical process but the main motivation of the model was to obtain a fit of the calcium-dependent whole-cell flux J_{IP_3R} to data collected by Parys et al. [58]. From a purely mathematical point of view, phenomenological models seem to be the ideal approach for investigating the role of IP_3R in calcium dynamics—restriction to minimal models that generate the desired behaviour ensures that model behaviour can be analysed to a great extent. This allows us to test hypotheses on IP_3R regulation in an elegant way.

But the capability of simple mathematical expressions for the macroscopic flux J_{IP_3R} to perform the appropriate functional role in calcium dynamics is only a relatively indirect test for IP_3R models. By following a phenomenological approach we mostly ignore data that gives more direct information on the IP_3R, such as, for example, the molecular structure of the channel protein which can be obtained from crystallography and time series of opening and closing of a single channel from patch-clamp recordings. Taking into account these data may allow us to restrict the set of theoretically possible mathematical expressions and, in this way, also the set of possible mechanism.

3. Data-driven modelling of single IP_3Rs

Because most biophysical data relate to single channels, data-driven modelling involves an important conceptual step—instead of directly specifying the whole-cell flux J_{IP_3R}, we first construct a model for the flux through a single channel. Whereas for the macroscopic flux J_{IP_3R} which is averaged spatially over many channels distributed across the whole cell the deterministic model (3) is appropriate, representing the flux through a single channel requires a stochastic model. In a second step, J_{IP_3R} is then derived by appropriately averaging over the stochastic fluxes through individual channels.

In Sections 3.1 and 3.2 we describe two sources of data that are commonly used for the construction of ion channel models. Ca^{2+} release data from small clusters of IP_3R, so-called calcium puffs (Section 3.3), can be used for validating models of single channels. In Section 3.4 aggregated continuous-time Markov models, the mathematical framework common to all models based on single-channel data, is introduced. A short review of statistical approaches for fitting Markov models to single-channel data is given in Section 3.5. In Sections 3.6 and 3.7 examples of two recent models of the IP_3R are given in order to illustrate different modelling approaches. Earlier models have been reviewed by [38] and Sneyd and Falcke [77]. Model comparisons [78, 40] generally show that models not parameterised by fitting to experimental data may not do a very good job at reproducing the statistical properties of ion channel kinetics.

3.1. **Molecular structure.**

The mathematical structure of many ion channel models is designed to mimic the chemical structure of the channel protein. The motivation for this approach is to link molecular structure of the ion channel to its function.

In vertebrates there exist three different genes encoding three different types of the IP_3R. In mammals, type I IP_3R is ubiquitously expressed but most cells express more than one isoform. The predominant isoform in astrocytes is type II IP_3R [69, 43]. For each isoform there are several splice variants.

Imaging the three-dimensional structure of the complete IP_3R and RyR channel proteins is challenging and only recently have accurate 3D visualisations of complete IP_3Rs using electron cryomicroscopy (cryo-EM) become available [49]. Parts of the channel can be imaged at higher resolution by crystallography and be superimposed on cryo-EM images [29]. These studies have revealed that IP_3R channels are tetramers i.e. formed by binding of four IP_3R proteins. These tetramers may consist of different IP_3R subtypes but experimental studies have so-far concentrated on investigating homotetramers formed by four copies of the same subtype (but see Alzayady et al. [2]). The classical description by De Young and Keizer [25] took into account this information by building a model from identical subunits that all had to be in an open state for the channel to open, although the model assumed three instead of four subunits.

Analysis of the amino acid sequence by mutation experiments have assigned functional roles to various segments, for example, the IP_3 binding core (IBC) which contains an IP_3 binding site has been identified. There is less information on the number and localisation of Ca^{2+} binding sites. Because localisation of Ca^{2+} binding sites by mutation studies has been difficult, Foskett et al. [31] infer various Ca^{2+} binding sensors from the observed co-regulation by IP_3 and Ca^{2+}, see Foskett and Mak [30] for a summary. Often models assume a certain number of IP_3 and Ca^{2+} binding sites and represent binding and unbinding of these ligands as transitions between states regulated by mass action kinetics. This modelling approach will be described in more detail in Section 3.6.

3.2. **Patch-clamp recordings.**

Detailed studies of individual ion channels became possible due to the development of the patch-clamp technique. Neher and Sakmann [56] were the first to detect the flow of ions through a single ion channel by measuring the resulting current at constant voltage. The time-course of opening and closing can be inferred from the detected

current which stochastically jumps between zero (closed) and one or more small non-zero current levels in the pA range (open) whose sign depends on the valence of the ion and the direction of the current.

Mak and Foskett [53] recently reviewed the single-channel literature of IP_3R channels. An important experimental development that they highlight relates to the difficulty that IP_3Rs are naturally localised within cells rather than in the cell membrane. Whereas in earlier patch-clamp experiments, IP_3R channels were studied in artificial lipid bilayers, more recently investigating IP_3R in isolated nuclei is favoured because it is assumed that nuclei provide an environment similar to the endoplasmic reticulum (ER), the native domain of the IP_3R.

3.2.1. *Stationary data.* If ligand concentrations (such as IP_3, Ca^{2+} and ATP) are kept constant for the whole duration of the experiment we obtain stationary data. These data allow us to observe the "typical" channel dynamics for a given combination of ligands. The reason that we refer to these data as "stationary" is that we assume that the channel has fully adjusted to the concentration of ligands—the term stationary suggests that the channel has reached its stationary probability distribution, see Section 3.4. Because the stationary solution is only reached asymptotically we can, in theory, never be sure that our ion channel has actually reached equilibrium. Instead we can check if a data set is *not* stationary by using indicators such as the open probability. If the open probability averaged over a sufficient number of data points spontaneously changes (which indicates the switching of the channel to a different activity level) the channel may exhibit modal gating.

3.2.2. *Modal gating.* Spontaneous switching between different levels of channel activity at constant ligand concentrations has been observed for a long time. The earliest example is perhaps from a classical study of the large-conductance potassium channel (BK) [52, 51]. In IP_3R channels modal gating was discovered only relatively recently [44]. The authors found three different modes characterised by high (H), intermediate (I) and low (L) levels of open probabilities, p_O^H, p_O^I and p_O^L. They also realised the importance of modal gating for IP_3R regulation: they observed that the same three modes seemed to exist for different combinations of ligand concentrations. Because the IP_3R mostly seemed to adjust the time spent in each of the three modes they proposed that modal gating is the major mechanism of ligand regulation in IP_3R channels.

One reason that the significance of modal gating has not been appreciated until recently is due to the fact that switching between different modes cannot always be recognised easily without statistical analysis. Recently, Siekmann et al. [72] developed a statistical method which for a given set of single-channel data detects switching between an arbitrary number of modes M^i characterised by their respective open probabilities $p_O^{M^i}$. A software implementation which is publicly available under `https://github.com/merlinthemagician/icmcstat.git` was applied to a large data set from Wagner and Yule [86]. Siekmann et al. [72] found that the same two modes, an inactive "park" ($p_O^{\text{park}} \approx 0$) and an active "drive" mode ($p_O^{\text{drive}} \approx 0.7$), were found across all combinations of ligands. There may be various reasons why two modes were observed rather than the three modes found in the earlier study [44], see Siekmann et al. [72] for more details. But more importantly, a detailed study of a bacterial potassium channel (KscA) [17, 16, 15] strongly suggests that the stochastic dynamics characteristic for each mode may be closely related to distinct three-dimensional configurations (conformations) of the channel. Thus, whereas it is often difficult to relate individual open or closed states in ion channel models to distinct conformations of the channel protein, the set of model states that represents a particular mode may, in fact, have a biophysical counterpart [72]. In order to confirm this hypothesis, more studies of modal gating for a variety of channels are needed.

Independent from its biophysical significance, appropriately accounting for modal gating is crucial from a modelling point of view. As we will see in Section 3.4, the phenomenon of modal

gating demonstrates that a Markov process must be observed for a sufficiently long time in order to infer the correct stationary distribution, otherwise we observe a "quasi-steady state". For example, a channel whose kinetics is restricted to an active and an inactive mode can produce intermediate activity only by switching between both modes. Thus, a model that is not capable of switching between different levels of activity is misleading because it produces a constant open probability instead of alternating between highly different open probabilities. In their recent review Mak and Foskett [53] explicitly recognise the importance of modal gating which so far has only been represented in the most recent models [84, 73].

3.2.3. *Response to rapid changes of ligand concentrations.* Modal gating is an aspect of stationary data collected at constant concentrations of ligands. In contrast, Mak et al. [54] designed an experiment where IP_3 and/or Ca^{2+} concentrations in the channel environment were rapidly altered in order to simulate an instantaneous change of ligand concentrations. Switching from ligand concentration where the IP_3R is inactive to conditions where the channel is maximally activated (and vice versa), enabled Mak et al. [54] to investigate the question how fast the IP_3R responds to varying ligand concentrations. To illustrate the experiment let us consider the change from inhibitory to activating conditions. At an inhibitory condition, the open probability of the channel is very close to zero ($p_O \approx 0$) so that initially the IP_3R is most likely closed. When changing from an inhibitory to an activating condition the channel will activate but it needs a certain time to respond to the change. In order to measure this latency, Mak et al. [54] recorded the time the channel took from when they altered the ligand concentration until the first opening. For the opposite change from activating to inhibitory conditions they analogously detected the time the channel needed to switch from a high to a low level of activity. This experiment was repeated multiple times for switching between the same conditions which enabled the authors to investigate the latency statistics. It was not only discovered that for some conditions the latencies were surprisingly long but interestingly, they also found that for some conditions the latency distributions were multi-modal which shows that multiple timescales may be observed for the same latency.

Due to the substantial effort required to perform these experiments (which have to be repeated multiple times for each condition where each repeat only gives a single data point rather than a time course) it is unsurprising that these data are very rare. In fact, to date, Mak et al. [54] is the only data set of this kind currently available. Mak and Foskett [53] explain that their data suggests that there may be long refractory periods between release events from the same IP_3R which makes these results particularly relevant for the modelling of Ca^{2+} puffs.

3.3. **Calcium puffs.** So far we have only considered data recorded from single IP_3Rs. In order to understand how the macroscopic flux J_{IP_3R} arises from the release of many individual channels we have to consider the hierarchical nature of Ca^{2+} release. As reviewed by Parker et al. [57], Falcke [28], Thurley et al. [80] stochastic opening of a single IP_3R channel leads to a localised Ca^{2+} release event (a Ca^{2+} blip). Such a release further sensitises neighbouring IP_3R to induce more Ca^{2+} release through a few tightly clustered IP_3Rs by CICR (a Ca^{2+} puff). Sufficiently many puffs could eventually trigger a global elevation of $[Ca^{2+}]_i$ that is able to propagate through the entire cell (a Ca^{2+} wave) [55]. Thus, Ca^{2+} puffs play a crucial role: not only are they essential for the formation of functional global Ca^{2+} signals [12] but they also reflect the quantal Ca^{2+} releases by stochastic openings of IP_3R *in vivo* [75].

Experimentally, Ca^{2+} release at a specific spatial position can be initiated by triggering release of caged IP_3 using a laser. A relative measure for the local Ca^{2+} concentration is obtained by detecting fluorescent dye bound to Ca^{2+} using a light microscope. For a given point within the cell the resulting time series is characterised by a sequence of stochastic spikes that are highly variable as far as the spike amplitude, the frequency and the time interval between subsequent spikes, the inter-puff interval, is concerned. From a modelling point of view, these

data can be used to test wether the single-channel behaviour represented in a model is able to account for the release from a cluster of interacting IP_3Rs. As explained in Section 4.1, Cao et al. [13] found that the original model by Siekmann et al. [73] was incapable of generating the correct stochastic puff distribution as long as the adaptation to different ligand concentrations was assumed to occur instantaneously. After augmenting the model so that it accounted for the latency data by Mak et al. [54] presented in the previous section the puff statistics could be reproduced accurately.

The only other model that accounts for latency data is the model by Ullah et al. [84]. Because the models by Siekmann et al. [73], Cao et al. [13] and by Ullah et al. [84] are the only models that account for all aspects of single-channel data assumed to be necessary for an understanding of the IP_3R we focus on these models and the alternative modelling approaches that they represent in Sections 3.6 and 3.7.

3.4. **Aggregated continuous-time Markov models.** The most natural model for the stochastic process of opening and closing of a single ion channel is the aggregated continuous-time Markov model. A good introduction to the theory reviewed here is the classical paper by Colquhoun and Hawkes [18] which also gives some simple but illustrative examples.

An aggregated continuous-time Markov model is a graph on a set of n_C closed and n_O open states $S = \{C_1, \dots, C_{n_C}, O_{n_C+1}, \dots, O_{n_C+n_O}\}$ (Figure 2).

Between adjacent states S_i and S_j the transition rate (from S_i to S_j) is given by $q_{ij} > 0$ so that the whole model is represented by a matrix with constant coefficients, the infinitesimal generator $\mathbf{Q} = (q_{ij})$. The time-dependent probability distribution $\mathbf{p}(t)$ over the state set S is the solution of the differential equation

$$\frac{d\mathbf{p}(t)}{dt} = \mathbf{p}(t)\mathbf{Q}, \qquad \mathbf{p}(0) = \mathbf{p}_0. \tag{5}$$

The stochastic interpretation of (5) is as follows: for a given point in time, one particular state S_i of the model is "active". But how long it will take until the current state S_i is vacated and which state S_j will be active after a time t cannot be answered with certainty (i.e. deterministically) due to the stochastic transitions between states.

For the model defined by (5) the Markov property holds both for the stochastic sequence of active states as well as for the time that it takes until the active state is left. In fact:

(1) which state S_j will be the next active state only depends on the currently active state S_i, not on previously active states.
(2) the time t_{S_i} it takes until the model exits from the state S_i, also called the *sojourn time* in S_i, does not depend on the time already spent in S_i.

The second point implies that sojourn times t_{S_i} must be exponentially-distributed because the exponential distribution is the only continuous probability distribution with this property. This explains why multiple open and closed states may be needed for accurately representing the opening and closing of ion channels.

In order to ensure that $\mathbf{p}(t)$ is a stochastic vector i.e. $\sum_{i=1}^{n_S} p_i,\ p_i \geq 0$ for all $t \geq 0$, the matrix $\mathbf{Q}$ must be conservative, i.e. for the diagonal elements q_{ii} we have

$$q_{ii} = -\sum_{j \neq i} q_{ij}, \qquad i, j = 1, \dots, n_S. \tag{6}$$

Provided that (6) holds, the solution

$$\mathbf{p}(t) = \mathbf{p}_0 \exp(\mathbf{Q}t), \tag{7}$$

is a stochastic vector for all $t > 0$ if and only if the initial distribution $\mathbf{p}_0$ is a stochastic vector. From (7) the time-dependent open probability $p_O(t)$ of the channel can be calculated by summing over the individual probabilities of all open states.

For large times t the solution $\mathbf{p}(t)$ approaches a stochastic vector $\boldsymbol{\pi}$ which is known as the stationary distribution. This means that provided we wait sufficiently long, the expected frequency of observing a state S_i approaches a probability π_i. Because $\mathbf{p}(t)$ is the solution of a differential equation, $\boldsymbol{\pi}$ is, in fact, a stationary solution of (5) i.e. can be obtained by solving the equation

$$\boldsymbol{\pi}\mathbf{Q} = 0. \tag{8}$$

This homogeneous linear equation has non-trivial solutions because the matrix $\mathbf{Q}$ is singular by (6). An argument based on Perron-Frobenius theory for non-negative matrices ensures that $\boldsymbol{\pi}$ is a unique strictly positive stochastic vector. Moreover, $\boldsymbol{\pi}$ is stable so that for $t \to \infty$ indeed $\mathbf{p}(t)$ approaches $\boldsymbol{\pi}$, i.e. we have $\lim_{t\to\infty} \mathbf{p}(t) = \boldsymbol{\pi}$ [68].

3.5. **Estimation of Markov models from experimental data.** Whereas the mathematical framework of aggregated Markov models was developed a short time after single channel data became available, the statistical estimation of these models is a topic of current research. Most commonly used are approaches based on Bayesian statistics. For a given time series Y of open and closed events recorded from an ion channel the conditional probability density $f(\mathbf{Q}|Y)$, known as the posterior density in the Bayesian framework, is used for determining a suitable Markov model with infinitesimal generator $\mathbf{Q}$. Note that both Y and $\mathbf{Q}$ are considered as random variables, thus the posterior distribution quantifies how likely a model $\mathbf{Q}$ is under the condition that data Y have been observed. Direct calculation of the posterior distribution $f(\mathbf{Q}|Y)$ is analytically intractable and computationally prohibitive but efficient approaches for maximum likelihood estimation (MLE) i.e. estimating

$$\hat{\mathbf{Q}} = \operatorname{argmax}_{\mathbf{Q}} f(\mathbf{Q}|Y) \tag{9}$$

were published in the 1990s [60, 61, 19]. Software implementations of these methods have been made available freely for academic use. Currently, the methods by Qin et al. [60, 61] can be obtained under the name `QUB` as standalone GUI applications at `http://www.qub.buffalo.edu/`. `DCPROGS` based on Colquhoun et al. [19] is still under active development and the source code of the most recent version has been published on github: `https://github.com/DCPROGS`.

An alternative approach to maximum likelihood estimation has been pursued since the late 1990s. The aim of Markov chain Monte Carlo (MCMC) is to approximate the posterior density $f(\mathbf{Q}|Y)$ by sampling. MCMC enables us to randomly generate a sequence $(\mathbf{Q}^k)_{k=1}^N$ of models such that the expected frequency of a model $\mathbf{Q}^k$ within this sequence is as large as the density $f(\mathbf{Q}^k|Y)$. Thus, by generating a sufficient number of samples, the posterior $f(\mathbf{Q}|Y)$ is approximated.

The early method by Ball et al. [4] for estimation of a Markov model $\mathbf{Q}$ depends on a suitable idealisation of discretely sampled measurements to continuous open and closed times. This leads to a difficult statistical problem that has been discussed widely in the ion channel literature as the "missed events" problem. Rosales and colleagues were the first to propose a method that directly uses the discrete measurements and thus does not require further idealisation of the data [65, 64]. Their algorithm estimates a discrete-time Markov model which describes the transition probabilities between states during a sampling interval rather than the so-called infinitesimal generator $\mathbf{Q}$. Gin et al. [36] were the first to propose a method for estimating $\mathbf{Q}$ from discretely-sampled data, their method was extended to models with arbitrary numbers of open and closed states by Siekmann et al. [74] and Siekmann et al. [70].

The current version of the software implementation of this method is available on github: https://github.com/merlinthemagician/ahmm.git. For an overview of various approaches to statistical modelling based on single-channel data, see Gin et al. [38].

The crucial advantage of MCMC methods over MLE approaches is that uncertainties can be comprehensively understood by analysing the posterior $f(\mathbf{Q}|Y)$. Already marginal distributions for individual rate constants (Figure 3) are helpful for localising and quantifying uncertainties within a model $\mathbf{Q}$.

But even more can be gained by analysing statistical relationships between combinations of model parameters as, for example, demonstrated by Siekmann et al. [70]. An important drawback of aggregated Markov models is non-identifiability i.e. model structures whose parameters cannot be inferred unambiguously from experimental data. Unfortunately, non-identifiable aggregated Markov models have not been completely classified [32, 33, 11]. But non-identifiability can at least be detected by analysing the posterior distribution $f(\mathbf{Q}|Y)$ [70]. Thus, MCMC allows us to disentangle different causes of model uncertainty because it enables us to distinguish between parameter uncertainties due to insufficient or noisy data from pathologies in the structure of the model itself.

3.6. **The Ullah et al. model.** A common approach for selecting a model structure for an ion channel model (which goes back at least to the classical model by De Young and Keizer [25]) is to identify the states of the Markov model with different chemical states of the channel protein. As explained in Section 3.1, the IP_3R has various binding sites that allow specific ligands such as Ca^{2+} and IP_3 to bind to the channel protein and induce conformational changes of its three-dimensional structure. To account for this, model states are distinguished by how many particles of each ligand are bound to the channel. This assumption not only determines the state set of the model but also the possible transitions between states—in each state we can either bind a ligand to a free binding site or remove a ligand from an occupied binding site. The dynamics of binding and unbinding of ligands is modelled by the law of mass action so that, in principle, the model is completely specified by the number of binding sites for each ligand. However, in practice, such a model would be heavily overparameterised when fitted to experimental data, so it is necessary to simplify the model.

To illustrate this with an example, consider the recent model by Ullah et al. [84] which is representative for this approach. The model states in Figure 2c are arranged in a grid whose coordinates are mapped by a two-digit subscript. The horizontal axis of the grid (left digit) show how many Ca^{2+} molecules are bound to the channel, whereas the vertical axis of the grid (right digit) indicates how many IP_3 binding sites are occupied, and whose columns. Thus, the position within the grid of a specific model state reflects how many Ca^{2+} ions and how many IP_3 molecules, respectively, are bound to the channel. For example, neither Ca^{2+} nor IP_3 are bound to the state C_{00}^{L} in the lower left corner whereas two Ca^{2+} and four IP_3 binding sites are occupied for the states C_{24}^{I}, O_{24}^{I}, C_{24}^{H} and O_{24}^{H}. This is also indicated by the subscript indices—the first digit stands for the number of Ca^{2+} ions whereas the second digit accounts for the number of IP_3 molecules bound to the channel. Figure 2c shows that only a subset of eight combinations, out of twenty possible combinations of occupying Ca^{2+}, ATP and IP_3 binding sites, appears in the model. This considerable reduction is due to the removal of "low occupancy states"—Ullah et al. [83] developed a perturbation theory approach that allows them to omit states with low stationary probabilities while at the same time accounting for the delays caused by passing through these states.

The model is constructed in an iterative four step process integrating several sources of data. In a first step, Ullah et al. [84] use Ca^{2+} and IP_3 dependency of the average open probability p_O in order to determine a minimal set of model states. By optimising an Akaike information criterion (AIC) score function, a model with five closed, C_{00}, C_{04}, C_{24}, C_{32} and C_{34}, and one open state, O_{24}, was selected as the best fit for the p_O data.

In a second step, the ligand-dependent average probabilities π^L, π^I and π^H of being in modes characterised by three different levels of activity as well as the open probabilities in each mode (p_O^L, p_O^I and p_O^H) are used for assigning each of the six model states with a mode. At this step, some additional states are added because, for example, the state C_{04} must exist both in the low (C_{04}^L) as well as the intermediate mode (C_{04}^L) in order to get a good fit to the data. To properly account for the Ca^{2+} dependency of p_O^I, the open probability in the intermediate mode, an additional state O_{14}^I had to be introduced.

In the first two steps, Ullah et al. [84] use stationary probabilities in order to determine which states should appear in the model without considering transitions between states. In step 3 the authors infer the transitions that are needed to account for the average sojourn times τ^L, τ^I and τ^H in the three modes whereas in step 4, data on the IP_3R response to rapid changes in Ca^{2+} and IP_3 (latencies) is used for determining the remaining transitions. Two additional states, C_{20}^L and C_{30}^L are introduced in order to account for the latency data.

Until this point, data is only used for determining the model structure but not for parameter estimation. The model is finally parameterised using the latency data from Mak et al. [54] or a combination of these data and single-channel time series obtained at three different constant Ca^{2+} concentrations.

3.7. **Siekmann et al. "Park-Drive" model.** The main aims of the modelling study by Siekmann et al. [73] were first to account for switching between an inactive "park" and an active "drive" mode observed in the data set by Wagner and Yule [86]. As mentioned by Mak et al. [54] and Foskett and Mak [30], Mak and Foskett [53], the importance of modal gating is well-recognised and the implications for not appropriately capturing the timescale separation of fast opening and closing and slower switching between different activity levels is obviously unsatisfactory from a modelling point of view.

Second, these data provided the possibility to build a model of two different mammalian isoforms of the IP_3R, type I and type II IP_3R. In addition to a comparative study of type I and type II IP_3R, these data also include ligand-dependency of ATP in addition to IP_3 and Ca^{2+}.

Third, Siekmann et al. [73] followed a primarily statistical approach to inference, rather than deriving the model from a binding scheme as the model by Ullah et al. [84] discussed above. Based on the experience of the earlier study by Gin et al. [37] where similar data could be fitted satisfactorily by a model with four states and only one ligand-dependent pair of rate constants, the number of parameters required to account for binding of IP_3, Ca^{2+} and ATP were likely to lead to a highly overparameterised model.

Due to these considerations, Siekmann et al. [73] made the inactive "park" and the active "drive" mode the construction principle of their model. In a first step, Markov models representing the stochastic dynamics for these two modes were constructed based on representative segments of the time series data that were characteristic for one of the two modes. Models with different numbers of states and model structures were fitted to these segments using the method by Siekmann et al. [74, 70]. It was observed that the best fits for either of the two modes across all combinations of ligands available in the large data set by Wagner and Yule [86] were quantitatively similar. In agreement with Ionescu et al. [44], this strongly suggested that the dynamics within park and drive modes are ligand-independent and that ligand-dependent regulation of IP_3R activity is achieved by varying the prevalence of park or drive mode.

In a second step after both park and drive mode had been modelled separately, a model of the ligand-dependent switching between the ligand-independent modes was constructed. The structure for the full Park-Drive model (Figure 2a) was found by connecting the Markov models of park and drive mode obtained previously with a pair of transition rates. Due to the infrequent switching between park and drive mode observed in the data it was decided that adding more than a single pair of transition rates was statistically unwarranted. The full Park-Drive model was then fitted to time series for all combinations of ligands of the study

by Wagner and Yule [86]. The results of these fits established the ligand-dependency of modal gating by the IP_3-, Ca^{2+}- and ATP-dependent variation of the two transition rates.

Probably the most important result of this study is that only models that take into account modal gating are able to accurately capture IP_3R kinetics. A channel whose kinetics is restricted to an active and an inactive mode can produce intermediate activity only by switching between both modes. Thus, a model that is not capable of switching between different levels of activity is misleading because it produces a constant open probability instead of alternating between highly different open probabilities. However, Cao et al. [13] showed that accounting for modal gating alone was insufficient for modelling stochastic Ca^{2+} release events (puffs) that arise from the interactions of a few IP_3R channels. This study showed that the Park-Drive model has to be augmented by latency data [54] in order to account for the delayed response of individual channels to changes in ligand concentrations.

Constructing the Park-Drive model based on the two modes proved very useful in the study by Cao et al. [14]. The authors iteratively reduced the Park-Drive model to a two-state model that only approximates the dynamics of opening and closing within the modes and focuses on the level of activity determined by the relative prevalence of the modes. This further emphasises that switching between park and drive mode rather than stochastic dynamics within the modes is the most important mechanism of IP_3R regulation.

3.8. **Comparison of type I and type II IP_3R.** The experimental study by Wagner and Yule [86] not only investigated the IP_3R under a wide range of ligand conditions but also contrasted the behaviour of type I and type II IP_3R. In the models for type I and type II IP_3R constructed by Siekmann et al. [73] at a first glance the similarities between both subtypes are probably more obvious than the differences. First of all, it is striking that both IP_3R subtypes can not only be represented in the same model structure but that active and inactive modes in both channels are nearly identical. This indicates that both subtypes have the same modes and that their differences are entirely due to differences in modal gating.

One difference is that type II IP_3R responds more sensitively to IP_3, in contrast to type I IP_3R. The most important differences between both subtypes was found to be ATP regulation, see Wagner and Yule [86], Siekmann et al. [73] for details.

4. Using data-driven IP_3R models in calcium dynamics

So far we have focused on the dynamics of individual IP_3Rs. In order to investigate the role of IP_3Rs in calcium dynamics we will now consider the interaction of IP_3Rs within a cluster.

4.1. **Modeling calcium puffs using the Park-Drive IP_3R model.** There is a large literature on stochastic models of calcium puffs for which we refer to the recent review by Rüdiger [66]. Here we present a simple model based on the Park-Drive model [73] which is based on the following assumptions:

- The ER contains sufficiently high $[Ca^{2+}]_i$ to keep a nearly constant Ca^{2+} release rate through a cluster of IP_3R [85]. Thus, ER $[Ca^{2+}]_i$ dynamics is not explicitly modeled.
- Ca^{2+} fluxes through the cell membrane have little effect on the very localised Ca^{2+} puffs far from cell membrane.
- We compartmentalise our model to capture heterogeneity within a cluster of IP_3Rs. We assume that sufficiently far away from individual channels we have a homogeneous basal Ca^{2+} concentration $c = [Ca^{2+}]_i$ that slowly responds to the total Ca^{2+} flux J_{IP_3R} through all IP_3R channels. In the vicinity of an open IP_3R channel this basal concentration c is elevated by a constant c_h; once the channel closes it instantaneously equilibrates to the basal concentration c.

Furthermore, Ca^{2+} buffers are not considered except a Ca^{2+} fluorescence dye. With these assumptions, the model is given as follows,

$$\frac{dc}{dt} = J_{IP_3R} + J_{leak} - \frac{V_d c}{c + K_d} - k_{on}(B - b)c + k_{off} b \tag{10}$$

$$\frac{db}{dt} = k_{on}(B - b)c - k_{off} b \tag{11}$$

where $V_d c/(c + K_d)$ models the flux (mainly via diffusion and SERCA) removing Ca^{2+} from the puff site. J_{leak} represents Ca^{2+} leak current from the ER for stabilising the resting $[Ca^{2+}]_i$ of $0.1\mu M$ (a typical value). B and b represent the total dye buffer concentration and Ca^{2+}-bound dye buffer concentration respectively, and the buffering process follows the mass action kinetics. J_{IP_3R} is the Ca^{2+} flux through open IP_3R, which is modeled by the production of a constant release flux rate (J_r) and number of open IP_3R channels (N_o), i.e. $J_{IP_3R} = J_r N_o$. Each open IP_3R will equally contribute to the elevation of cluster $[Ca^{2+}]_i$, c. Note that the actual $[Ca^{2+}]_i$ modulating each IP_3R is either c, when the receptor is in closed states, or $c + c_h$, when it is in open states. Parameters values are $J_r = 200\,\mu M$, $V_d = 4000\,\mu M s^{-1}$, $K_d = 12\,\mu M$, $J_{leak} = 33\,\mu M s^{-1}$, $B = 20\,\mu M$, $k_{on} = 150\,\mu M s^{-1}$, $k_{off} = 300\,s^{-1}$ and $c_h = 120\,\mu M$ [13]. The cluster is assumed to contain 10 IP_3R channels.

The Park-Drive IP_3R model is used to simulate IP_3R state and coupled to the deterministic equations via a hybrid-Gillespie method [67]. However, the puff model based on the Park-Drive model fails to reproduce nonexponential interpuff interval (IPI) distribution due to the sole use of stationary single channel data (i.e. Ca^{2+} is fixed during measurement) in IP_3R model construction. This does not allow the model to capture the transient single channel behaviour when Ca^{2+} experiences a rapid change [54, 13]. Thus, the Park-Drive model is modified by incorporating time-dependent inter-mode transitions so that the transient single channel behaviour is captured. In detail, the transition rates q_{24} and q_{42} are changed from constants to functions of four newly-introduced gating variables,

$$q_{24} = a_{24} + V_{24}(1 - m_{24}h_{24}) \tag{12}$$

$$q_{42} = a_{42} + V_{42} m_{42} h_{42} \tag{13}$$

where m_{24}, h_{24}, m_{42} and h_{42} are gating variables obeying

$$\frac{dG}{dt} = \lambda_G(G_\infty - G),\ G = m_{24}, h_{24}, m_{42}, h_{42}. \tag{14}$$

G_∞ is the steady state which is a function of channel-sensed Ca^{2+} and IP_3 concentrations and is determined by stationary single channel data (i.e. the Park-Drive model). λ_G is the rate at which the steady state is approached. This is based on the fact that a IP_3R channel cannot immediately reach its steady state upon a transient change in Ca^{2+} concentration [54]. The values of λ_G for m_{24}, h_{24} and m_{42} are found to be large so that the three gating variables could be approximated by their steady states i.e. $G = G_\infty$, a method called quasi-steady-state approximation. However, $\lambda_{h_{42}}$ at low $[Ca^{2+}]_i$ should be very small, reflecting a very slow recovery of IP_3R from high Ca^{2+} inhibition [54]. Note that when $\lambda_{h_{42}}$ is sufficiently large, quasi-steady-state approximation applies and the modified IP_3R model reduces to the original Park-Drive model. Details about the functions and parameters can be seen in [13].

An example of simulation results using the modified Park-Drive model is given in Figure 4. The waiting time between two successive puffs (or interpuff interval, IPI) is a key statistics to quantify the underlying process governing the emergence of puffs. Figure 5 shows that, as $\lambda_{h_{42}}$ at low $[Ca^{2+}]_i$ increases, the IPI distribution changes from nonexponential to exponential, demonstrating that the missing slow time scale in the original Park-Drive model is very crucial to explain the inhomogeneous Poisson process governing puff emergence found by (Thurley

et al. [81]). The IPI distributions were generated by fitting the probability density function proposed by Thurley et al. [81] to the simulated IPI histograms [13]. The proposed IPI distribution is

$$P = \lambda(1 - e^{-\xi t})e^{[-\lambda t + \lambda(1-e^{-\xi t})/\xi]}, \tag{15}$$

where t represent IPI. λ is the puff rate, a measure of the typical IPI (similar to average puff frequency), and ξ is the recovery rate.

Hence, this example shows the particular importance of considering both stationary and nonstationary data when constructing an IP_3R model. However, even if a model is constructed based on both data sets, it could also fail to reproduce Ca^{2+} puffs. One example is the Ullah model [84] as introduced in Section 3.6. A model simulation using the same puff model (10), (11) with the Ullah model is given in Fig. 6 where the Ca^{2+} signal behaves very irregularly and no puffs are clearly detected.

4.2. **The role of modal gating of IP_3R in modulating calcium signals.** The Park-Drive model (and its modified version) has the feature that IP_3R exist in two different modes, each of which contains multiple states, some open, some closed. Intermode transitions are important for modulating Ca^{2+} signals because of their ligand- and time-dependent property. However, structure within each mode may also have substantial contribution to the formation of different Ca^{2+} signals. Here, we examine the relative importance of intermode and intramode transitions using model reduction methods. By reducing the 6-state IP_3R model to a 2-state open/closed model, we will remove the intramodal structure, and a direct comparison between the statistics generated by the two IP_3R models will show the importance of intramodal structure.

The model reduction takes the following steps:

- The low probabilities of C_1 , C_3 and O_5 (sum of which is less than 0.03 for any $[Ca^{2+}]_i$) means that the IP_3R either rarely visit those states or have very short dwell time in those states. This allows to completely remove the three states from the 6-state model.
- Transitions q_{26} and q_{62} are far larger (about two orders of magnitude) than q_{24} and q_{42}. By taking a quasi-steady state approximation to the transition between C_2 and O_6, we have $O_6 = C_2 q_{26}/q_{62}$. Combining C_2 and O_6 to be a new state D, i.e. $D = C_2 + O_6$, the 6-state model becomes a 2-state model, where D represents a partially open state with Ca^{2+} flux through the channel decreased by a factor of $q_{26}/(q_{62} + q_{26})$. Moreover, q_{24} needs to be rescaled by $q_{62}/(q_{62} + q_{26})$ due to the quasi-steady state approximation so that the effective closing rate is $q_{24}q_{62}/(q_{62} + q_{26})$.

For model simulations, the state of each IP_3R is determined by the reduced IP_3R model and the equations governing the cytoplasmic calcium concentration and the calcium dye buffer remain Eqs. (10) and (11) except that calcium flux J_r is replaced by $q_{26}/(q_{26} + q_{62}) \cdot J_r$. Parameter values remain unchanged (Table).

Figure 7 shows the distributions of interpuff interval, puff duration and amplitude generated by using the 6-state IP_3R model (the Park-Drive model) and the reduced 2-state model. Reducing the intramodal structure does not qualitatively change the distributions but may lead to quantitative difference, which could be caused by missing open state O_5 that significantly contributes to the fluctuations of basal level of $[Ca^{2+}]_i$. However, if the IP_3R channel is not very sensitive to small fluctuations of basal $[Ca^{2+}]_i$, the quantitative difference is significantly reduced [14]. Thus, the fundamental process governing the generation of Ca^{2+} puffs and oscillations is primarily controlled by the modal structure but not the intramodal structure which improves the model fitting to the single-channel data.

5. Conclusions

The IP_3R plays a major role in CICR. For this reason, more and more aspects of its behaviour have been investigated by experiments. It usually turned out that new types of data had to be explicitly included in a model to account for them. For example, in early models such as the De Young-Keizer model [25], the rate constants were determined by fitting to the p_O observed at different calcium concentrations. But it soon became obvious that models parameterised with p_O data could not be used for extrapolating the channel kinetics, i.e. the stochastic opening and closing. See Sneyd and Falcke [77] or Ullah et al. [84] for a more detailed explanation why it is impossible to infer kinetics from the ligand dependency of the open probability p_O.

Just as kinetics cannot be inferred from p_O it turned out that the response of the IP_3R to varying ligand concentrations cannot be predicted from data collected at constant ligand concentrations. This was demonstrated by the next generation of models that were directly fitted to single-channel data, taking into account the stochastic process of opening and closing. The simplest assumption for integrating models for different ligand concentration is that the IP_3R adjusts instantaneously. If this were true in practice, we could represent the channel kinetics appropriately by simply replacing the model for the kinetics at 0.05 µM with the model for the kinetics at 0.2 µM calcium as we increase the calcium concentration. But Cao et al. [13] showed that only after taking into account rapid-perfusion data generated by Mak et al. [54] was the model of Siekmann et al. [73] capable of generating the correct puff distribution.

It is important to note that taking into account more data does not necessarily have to lead to more complicated models. Instead, after taking into account that the simpler kinetics of modal gating should capture the part of the channel dynamics that is most important for the functional role of the IP_3R in CICR, Cao et al. [14] were able to reduce the six-state model by Siekmann et al. [73] to a two-state model. Thus, after interpreting experimental data in the right way, we are able to build models for the functional role of IP_3R that are nearly as simple as the early phenomenological models.

6. Future work

After reviewing the current state of data-driven approaches to investigating the IP_3R we would like to take a look at promising future directions. In order to address the particular importance of modal gating, Siekmann et al. [71] develop a novel hierarchical model structure that enables us to combine Markov models that represent the stochastic switching between modes with models that account for the characteristic opening and closing within different modes. Thus, models for both processes can be fitted separately (e.g. using the method by Siekmann et al. [74, 70]) after analysing the data with statistical method presented by Siekmann et al. [72]. This allows us to build models for modal gating following a completely data-driven approach.

More generally, we have compared two current models as representative examples for different modelling approaches, the Ullah et al. [84] and the Park-Drive model [73, 13, 14]. Although both approaches ultimately meet in the middle, their different construction principles impose different requirements for future progress. From a statistical point of view, representation of ligand interactions with a channel by mass action kinetics as in Ullah et al. [84] defines a sufficiently large search space of models. It is crucial to select from this search space an appropriately simplified model that is obtained by removing states of the full model in a consistent way. A method for model reduction is provided by Ullah et al. [83] and Ullah et al. [84] demonstrate how data can be used to statistically select from all possible simplified models. A central principle of the biophysical approach is to design models in a way that closely follows physical principles. In this context, the bond-graph approach to modelling ion channels by Gawthrop and Crampin [34], Gawthrop et al. [35] is highly relevant because it ensures that physical principles are enforced when choosing a model structure.

For models that primarily focus on a statistically satisfying representation in a first instance, the model selection problem arises again but in the other direction. Rather than starting from a model structure determined by an underlying mass action model, Gin et al. [37] and Siekmann et al. [73] iteratively increased the number of states in their model structure until further increasing the number of parameters appears statistically unwarranted. This process is time-consuming and may be computationally prohibitive if models exceed a certain number of states. Developing a method that is able to automatically compare models with an increasing number of states has proven to be difficult, as indicated by the few number of studies that have appeared on this subject after an early article on comparison of a finite number of models [41]. A promising new direction is the non-parametric Bayesian method developed by Hines et al. [39] which allows the authors to estimate the number of states within an ion-channel data set. Determining the required number of open and closed states in a first step may increase efficiency because it restricts the class of models which have to be compared in a second step.

ACKNOWLEDGEMENTS

Funding from NIH grant R01-DE19245 is gratefully acknowledged.

TABLE 1. Model parameters. IP_3-dependent parameters are evaluated at a concentration of 0.1 µM as indicated by subscripts. Full model details are given in Cao et al. [13].

Symbol	Description	Value	Units
	Gating kinetics		
a_{24}	Basal level of q_{24}	$29.85_{p=0.1\,\mu M}$	s^{-1}
V_{24}	Gating-dependent part of q_{24}	$312.85_{p=0.1\,\mu M}$	s^{-1}
a_{42}	Basal level of q_{42}	$0.05_{p=0.1\,\mu M}$	s^{-1}
V_{42}	Gating-dependent part of q_{42}	100	s^{-1}
$\lambda_{h_{24}}$	Rate of approach to steady state of h_{24}	40	s^{-1}
n_{-24}	Hill coefficient for Ca^{2+} dependency of $h_{24\infty}$	$0.04_{p=0.1\,\mu M}$	
k_{-24}	Half-saturation constant for Ca^{2+} dependency of $h_{24\infty}$	$97.00_{p=0.1\,\mu M}$	
$h_{24\infty}$	Steady state of h_{24}	$\frac{k_{-24}^{n_{-24}}}{c^{n_{-24}}+k_{-24}^{n_{-24}}}$	
$a_{h_{42}}$	Basal level of $\lambda_{h_{42}}$ (tuning parameter)	0.5	s^{-1}
$V_{h_{42}}$	Ca^{2+}-dependent part of $\lambda_{h_{42}}$	100	s^{-1}
$K_{h_{42}}$	Half-saturation constant for Ca^{2+}-dependency of $\lambda_{h_{42}}$	20	µM
$\lambda_{h_{42}}$	Rate of approach to steady state of h_{42}	$a_{h_{42}}+\frac{V_{h_{42}}c^7}{c^7+K_{h_{42}}^7}$	s^{-1}
n_{-42}	Hill coefficient for Ca^{2+} dependency of $h_{42\infty}$	$3.23_{p=0.1\,\mu M}$	
k_{-42}	Half-saturation constant for Ca^{2+} dependency of $h_{42\infty}$	$0.17_{p=0.1\,\mu M}$	
$h_{42\infty}$	Steady state of h_{42}	$\frac{k_{-42}^{n_{-42}}}{c^{n_{-42}}+k_{-42}^{n_{-42}}}$	
$\lambda_{m_{24}}$	Rate of approach to steady state of m_{24}	100	s^{-1}
n_{24}	Hill coefficient for Ca^{2+} dependency of $m_{24\infty}$	$6.31_{p=0.1\,\mu M}$	
k_{24}	Half-saturation constant for Ca^{2+} dependency of $m_{24\infty}$	$0.549_{p=0.1\,\mu M}$	
$m_{24\infty}$	Steady state of m_{24}	$\frac{c^{n_{24}}}{c^{n_{24}}+k_{24}^{n_{24}}}$	
$\lambda_{m_{42}}$	Rate of approach to steady state of m_{42}	100	s^{-1}
n_{42}	Hill coefficient for Ca^{2+} dependency of $m_{42\infty}$	$11.16_{p=0.1\,\mu M}$	
k_{42}	Half-saturation constant for Ca^{2+} dependency of $m_{42\infty}$	$0.40_{p=0.1\,\mu M}$	
$m_{42\infty}$	Steady state of m_{42}	$\frac{c^{n_{42}}}{c^{n_{42}}+k_{42}^{n_{42}}}$	
	Ca^{2+} balance		
c_h	Elevated Ca^{2+} in vicinity of open IP_3R channel	120	µM
B	Total buffer concentration	20	µM
k_{on}	Binding of fluo4 buffer to Ca^{2+}	150	$\mu M s^{-1}$
k_{off}	Unbinding of fluo4 buffer from Ca^{2+}	300	s^{-1}
J_r	Flux of Ca^{2+} through single channel	200	$\mu M s^{-1}$
J_{leak}	Ca^{2+} influx from cluster environment	33	$\mu M s^{-1}$
V_d	Rate of cytoplasmic Ca^{2+} removal from the cluster	4000	$\mu M s^{-1}$
K_d	Half-saturation constant for cytoplasmic Ca^{2+} removal	12	µM

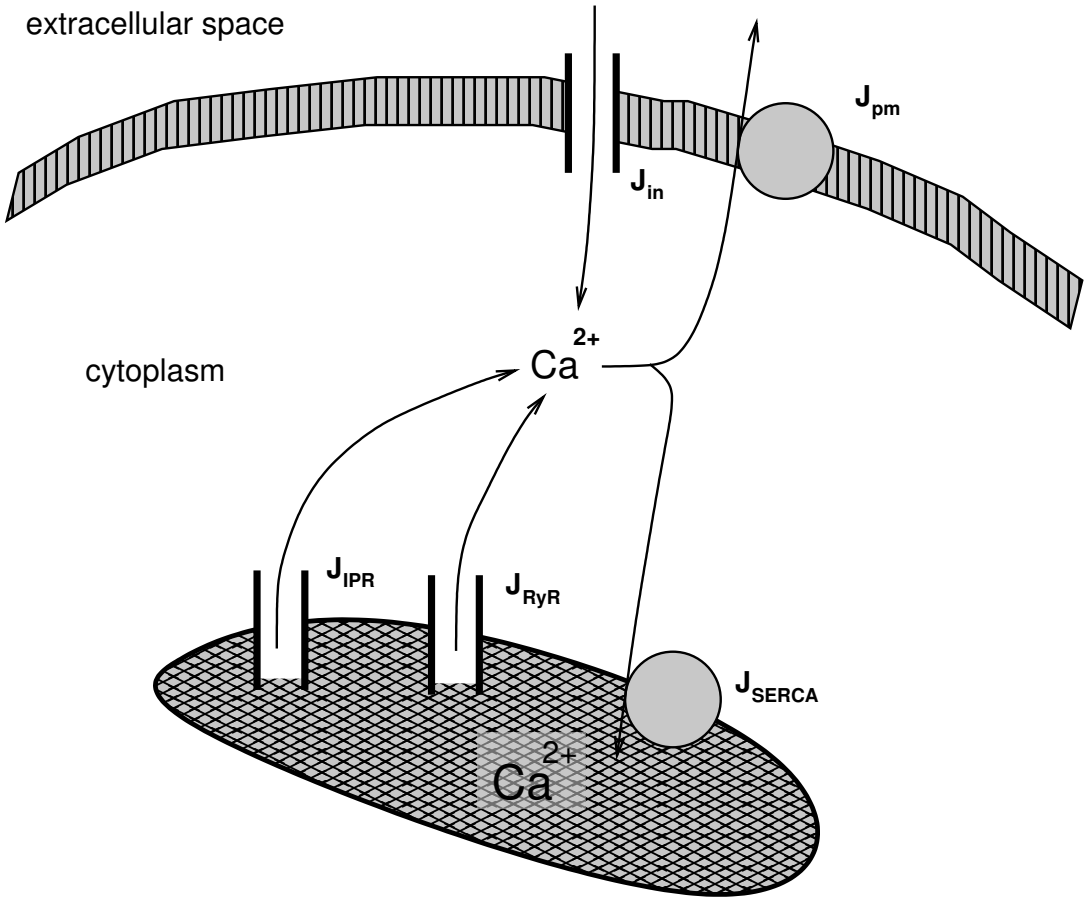

FIGURE 1. General structure of calcium fluxes in glial (and other non-excitable) cells. The central component is the flux J_{IPR} through the inositol trisphosphate receptor (IP_3R). The IP_3R is activated by binding of IP_3 which is generated upon stimulation of the cell by an agonist. This causes the release of Ca^{2+} from the endoplasmic reticulum (ER) to the cytoplasm. The resulting elevated Ca^{2+} concentration increases the open probability of the IP_3R and the ryanodine receptor (RyR) which stimulates further Ca^{2+} release. This mechanism is known as calcium induced calcium release (CICR). At high concentrations, Ca^{2+} inhibits the IP_3R, i.e. the open probability of the IP_3R decreases. In consequence, J_{SERCA} influx into the ER through the SERCA pump dominates the efflux through IP_3R and RyR so that Ca^{2+} is reabsorbed by the ER. Ca^{2+} exchange with the extracellular space is controlled by uptake through various channels (J_{in}) and by extrusion via pumps (J_{pm}).

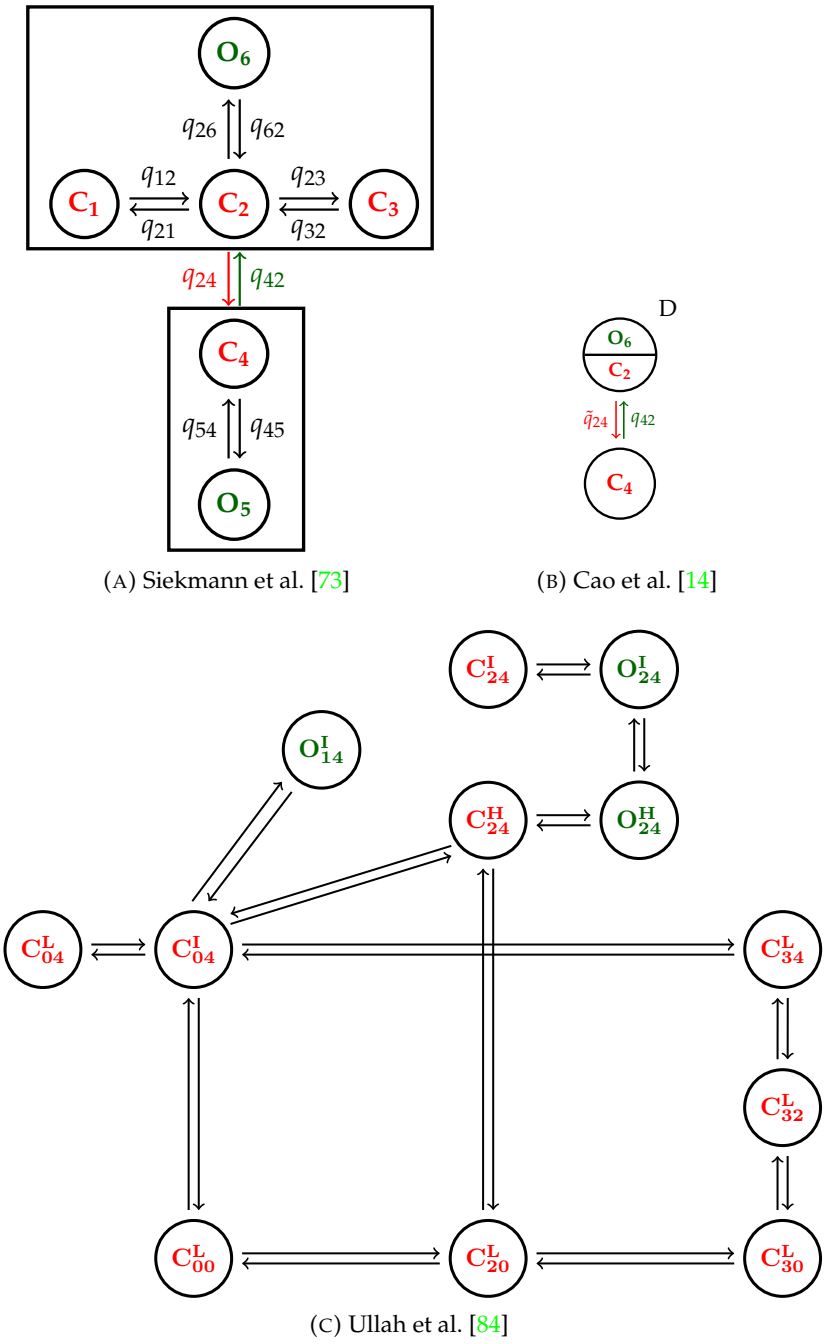

(A) Siekmann et al. [73]

(B) Cao et al. [14]

(C) Ullah et al. [84]

FIGURE 2. Two examples of recent Markov models of the IP_3R. Two versions of the Park-Drive model are shown in (A) and (B) whereas the model by Ullah et al. [84] is shown in (C). The original six-state Park-Drive model (A) by Siekmann et al. [73] has been simplified by Cao et al. [14] to a two-state model (B). As described in more detail in the main text, C_1, C_3 and O_5 were omitted due to their low occupancy. The two states C_2 and O_6 of the Drive mode were approximated by a partially open state D which releases a ratio of $\frac{q_{26}}{q_{26}+q_{62}}$ of the flux J_r assumed to flow through a single channel. Due to the altered occupancy of the state D the rate q_{24} must be corrected by the scaling factor so that we obtain $\tilde{q}_{24} = q_{24}\frac{q_{62}}{q_{26}+q_{62}}$.

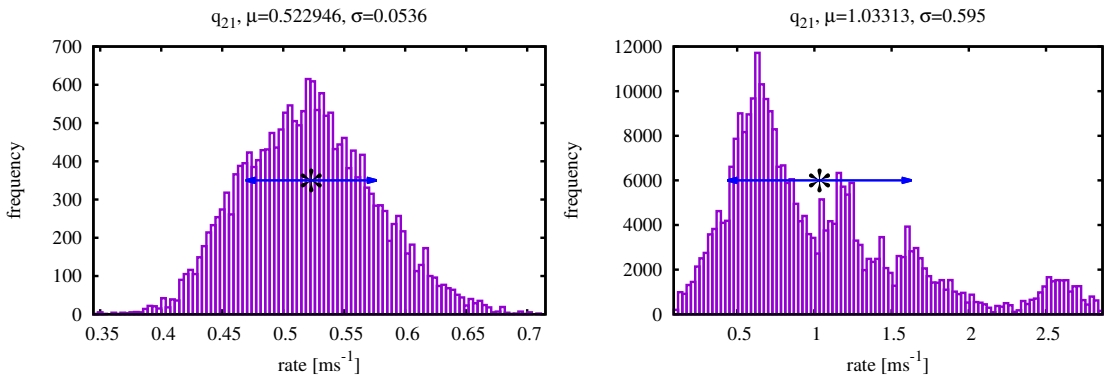

FIGURE 3. Two examples for marginal distributions of rate constants. (a) shows a histogram with a well-defined mean μ and a low standard deviation σ which indicates a low level of parameter uncertainty whereas the histogram in (b) shows a complex multi-modal distribution which shows that multiple values of the rate constants are capable of representing the data.

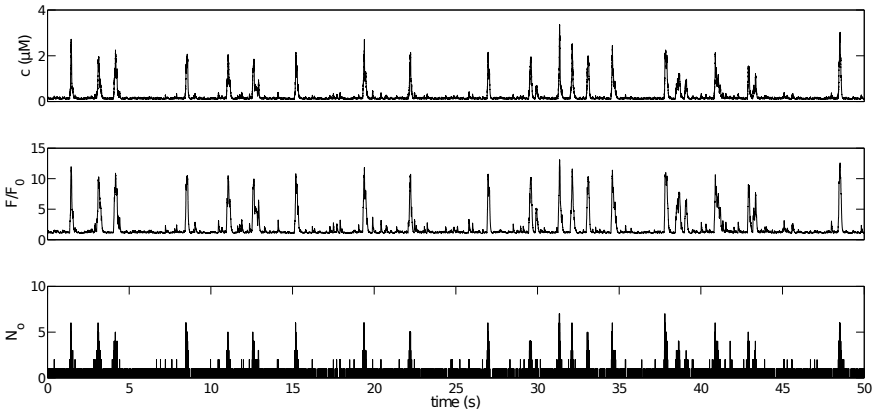

FIGURE 4. A simulation result of calcium puffs. F/F_0 represents the ratio of Ca^{2+}-bound dye buffer b to its resting value. IP_3 concentration is 0.1 μM. Adapted from [13].

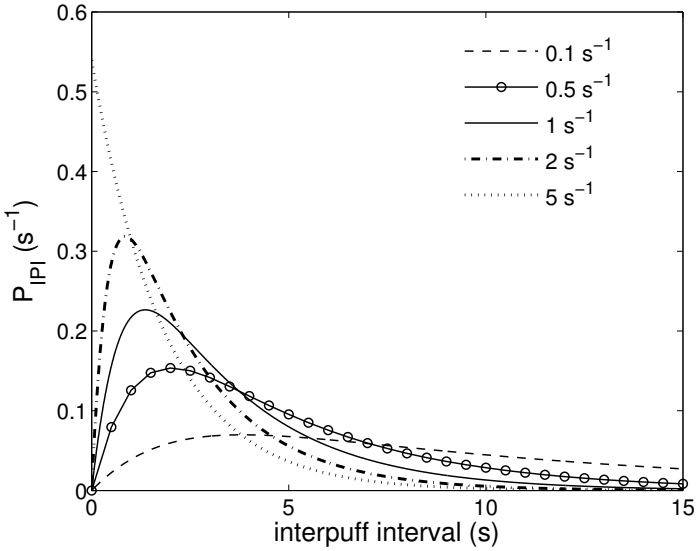

FIGURE 5. Dependence of IPI distribution on $\lambda_{h_{42}}$ (indicated in the legend) at low $[Ca^{2+}]_i$. IP_3 concentration is 0.1 μM. Adopted from [13].

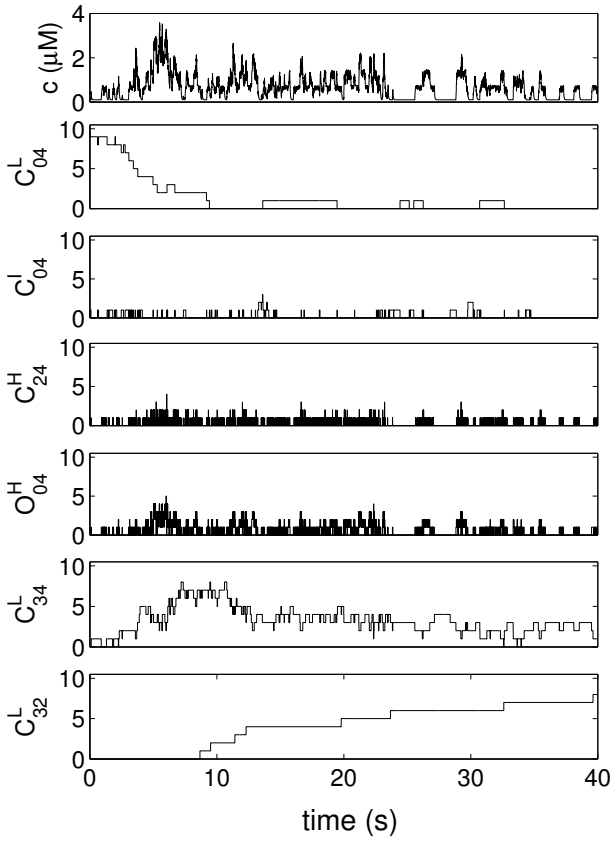

FIGURE 6. A simulation result of calcium puffs using the Ullah IP_3R model. IP_3 concentration is $0.1\mu M$. y-axis values indicate the number of IP_3R channels in corresponding states. Parameter values for the puff model remain the same.

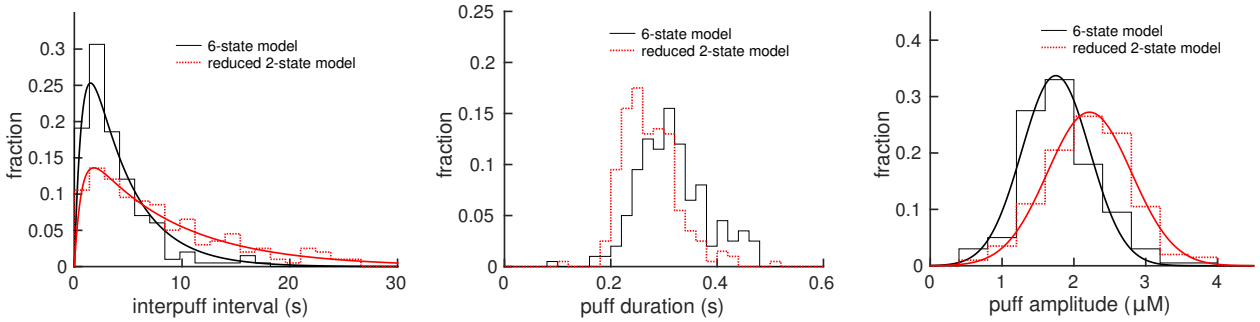

(A) (B) (C)

FIGURE 7. Comparison of interpuff interval, puff duration and amplitude between the 6-state IP_3R model (the Park-Drive model) and the reduced 2-state model. 199 samples for each model were used to generate **A** and 200 samples for **B** and **C**. Interpuff interval distributions were fit by using Eq.15 proposed by Thurley et al. [81]. Puff amplitude distributions were fit by normal distribution.

REFERENCES

[1] Allegrini, P., L. Fronzoni, and D. Pirino (2009). The influence of the astrocyte field on neuronal dynamics and synchronization. *Journal of Biological Physics 35*(4), 413–423. cited By 12.

[2] Alzayady, K. J., L. E. Wagner, R. Chandrasekhar, A. Monteagudo, R. Godiska, G. G. Tall, S. K. Joseph, and D. I. Yule (2013). Functional inositol 1,4,5-trisphosphate receptors assembled from concatenated homo- and heteromeric subunits. *Journal of Biological Chemistry 288*(41), 29772–29784.

[3] Atri, A., J. Amundson, D. Clapham, and J. Sneyd (1993). A single-pool model for intracellular calcium oscillations and waves in the Xenopus laevis oocyte. *Biophysical Journal 65*(4), 1727–1739.

[4] Ball, F. G., Y. Cai, J. B. Kadane, and A. O'Hagan (1999). Bayesian inference for ion-channel gating mechanisms directly from single-channel recordings, using Markov chain Monte Carlo. *Proceedings of the Royal Society of London A 455*, 2879–2932.

[5] Barrack, D. S., R. Thul, and M. R. Owen (2014). Modelling the coupling between intracellular calcium release and the cell cycle during cortical brain development. *Journal of Theoretical Biology 347*, 17–32.

[6] Barrack, D. S., R. Thul, and M. R. Owen (2015). Modelling cell cycle synchronisation in networks of coupled radial glial cells. *Journal of Theoretical Biology 377*, 85–97.

[7] Bennett, M. R., V. Buljan, L. Farnell, and W. G. Gibson (2006). Purinergic junctional transmission and propagation of calcium waves in spinal cord astrocyte networks. *Biophysical Journal 91*, 3560–3571.

[8] Bennett, M. R., L. Farnell, and W. G. Gibson (2005). A quantitative model of purinergic junctional transmission of calcium waves in astrocyte networks. *Biophysical Journal 89*, 2235–2250.

[9] Bennett, M. R., L. Farnell, and W. G. Gibson (2008). A quantitative model of cortical spreading depression due to purinergic and gap-junction transmission in astrocyte networks. *Biophysical Journal 95*, 5648–5660.

[10] Bezprozvanny, I., J. Watras, and B. E. Ehrlich (1991). Bell-shaped calcium-response curves of Ins(1,4,5)P_3-gated and calcium-gated channels from endoplasmic-reticulum of cerebellum. *Nature 351*(6329), 751–754.

[11] Bruno, W. J., J. Yang, and J. E. Pearson (2005). Using independent open-to-closed transitions to simplify aggregated Markov models for ion channel gating kinetics. *Proceedings of the National Academy of Science of the United States of America 102*(16), 6326–6331.

[12] Callamaras, N., J. S. Marchant, X. P. Sun, and I. Parker (1998). Activation and coordination of $InsP_3$-mediated elementary Ca^{2+} events during global Ca^{2+} signals in xenopus oocytes. *Journal of Physiology 509*, 81–91.

[13] Cao, P., G. Donovan, M. Falcke, and J. Sneyd (2013). A stochastic model of calcium puffs based on single-channel data. *Biophysical Journal 105*, 1133–1142.

[14] Cao, P., X. Tan, G. Donovan, M. J. Sanderson, and J. Sneyd (2014, 08). A deterministic model predicts the properties of stochastic calcium oscillations in airway smooth muscle cells. *PLoS Computational Biology 10*(8), e1003783.

[15] Chakrapani, S., J. F. Cordero-Morales, V. Jogini, A. C. Pan, D. M. Cortes, B. Roux, and E. Perozo (2011). On the structural basis of modal gating behaviour in K^+ channels. *Nature Structural and Molecular Biology 18*(1), 67–75.

[16] Chakrapani, S., J. F. Cordero-Morales, and E. Peroso (2007). A quantitative description of KscA gating II: Single-channel currents. *Journal of General Physiology 130*(5), 479–496.

[17] Chakrapani, S., J. F. Cordero-Morales, and E. Perozo (2007). A quantitative description of KscA gating I: Macroscopic currents. *Journal of General Physiology 130*(5), 465–478.

[18] Colquhoun, D. and A. G. Hawkes (1981). On the stochastic properties of single ion channels. *Proceedings of the Royal Society of London B 211*, 205–235.

[19] Colquhoun, D., A. G. Hawkes, and K. Srodzinski (1996). Joint distributions of apparent open and shut times of single-ion channels and maximum likelihood fitting of mechanisms. *Philosophical Transactions of the Royal Society of London A 354*, 2555–2590.

[20] De Pittà, M., M. Goldberg, V. Volman, H. Berry, and E. Ben-Jacob (2009). Glutamate regulation of calcium and ip3 oscillating and pulsating dynamics in astrocytes. *Journal of Biological Physics 35*(4), 383–411. cited By 26.

[21] De Pittà, M., V. Volman, H. Berry, and E. Ben-Jacob (2011, 12). A tale of two stories: Astrocyte regulation of synaptic depression and facilitation. *PLoS Comput Biol 7*(12), e1002293.

[22] De Pittà, M., V. Volman, H. Berry, V. Parpura, A. Volterra, and E. Ben-Jacob (2012). Computational quest for understanding the role of astrocyte signaling in synaptic transmission and plasticity. *Frontiers in Computational Neuroscience 6*, 98. cited By 0.

[23] De Pittà, M., V. Volman, H. Levine, and E. Ben-Jacob (2009). Multimodal encoding in a simplified model of intracellular calcium signaling. *Cognitive Processing 10*(1), 55–70.

[24] De Pittà, M., V. Volman, H. Levine, G. Pioggia, D. De Rossi, and E. Ben-Jacob (2008). Coexistence of amplitude and frequency modulations in intracellular calcium dynamics. *Physical Review E - Statistical, Nonlinear, and Soft Matter Physics 77*(3), 030903. cited By 30.

[25] De Young, G. W. and J. Keizer (1992). A single-pool inositol 1,4,5-trisphosphate-receptor-based model for agonist-stimulated oscillations in Ca^{2+} concentration. *Proceedings of the National Academy of Sciences 89*(20), 9895–9899.

[26] Dupont, G., E. F. L. Lokenye, and R. J. Challiss (2011). A model for ca2+ oscillations stimulated by the type 5 metabotropic glutamate receptor: An unusual mechanism based on repetitive, reversible phosphorylation of the receptor. *Biochimie 93*(12), 2132 – 2138. The Calcium signal: a universal carrier to code, decode and transduce information.

[27] Edwards, J. and W. Gibson (2010). A model for ca2+ waves in networks of glial cells incorporating both intercellular and extracellular communication pathways. *Journal of Theoretical Biology 263*(1), 45–58. cited By 0.

[28] Falcke, M. (2004). Reading the patterns in living cells – the physics of Ca^{2+} signaling. *Advances in Physics 53*(3), 255–440.

[29] Fedorenko, O. A., E. Popugaeva, M. Enomoto, P. B. Stathopulos, M. Ikura, and I. Bezprozvanny (2014). Intracellular calcium channels: Inositol-1,4,5-trisphosphate receptors. *European Journal of Pharmacology 739*, 39 – 48. Special Issue on Calcium Channels.

[30] Foskett, J. K. and D.-O. D. Mak (2010). Regulation of {IP3R} channel gating by ca2+ and ca2+ binding proteins. In I. I. Serysheva (Ed.), *Structure and Function of Calcium Release Channels*, Volume 66 of *Current Topics in Membranes*, pp. 235 – 272. Academic Press.

[31] Foskett, J. K., C. White, K. Cheung, and D. Mak (2007). Inositol trisphosphate receptor Ca^{2+} release channels. *Physiological Reviews 87*, 593–568.

[32] Fredkin, D. R., M. Montal, and J. A. Rice (1985). Identification of aggregated Markovian models: Application to the nicotinic acetylcholine receptor. In L. M. L. Cam and R. A. Olshen (Eds.), *Proceedings of the Berkeley Conference in Honor of Jerzy Neyman and Jack Kiefer*, Volume 1, Belmont, CA, pp. 269–289. Wadsworth.

[33] Fredkin, D. R. and J. A. Rice (1986). On aggregated Markov processes. *Journal of Applied Probability 23*(1), 208–214.

[34] Gawthrop, P. J. and E. J. Crampin (2014). Energy-based analysis of biochemical cycles using bond graphs. *Proceedings of the Royal Society of London A: Mathematical, Physical and Engineering Sciences 470*(2171), 20140459.

[35] Gawthrop, P. J., J. Cursons, and E. J. Crampin (2015). Hierarchical bond graph modelling of biochemical networks. *Proceedings of the Royal Society A: Mathematical, Physical and Engineering Sciences 471*(2184)), 1–23.

[36] Gin, E., M. Falcke, L. E. Wagner, D. I. Yule, and J. Sneyd (2009). Markov chain Monte Carlo fitting of single-channel data from inositol trisphosphate receptors. *Journal of Theoretical Biology 257*, 460–474.

[37] Gin, E., M. Falcke, L. E. Wagner II, D. I. Yule, and J. Sneyd (2009). A kinetic model of the inositol trisphosphate receptor based on single-channel data. *Biophysical Journal 96*(10), 4053–4062.

[38] Gin, E., L. E. Wagner II, D. I. Yule, and J. Sneyd (2009). Inositol trisphosphate receptor and ion channel models based on single-channel data. *Chaos: An Interdisciplinary Journal of Nonlinear Science 19*(3), 037104.

[39] Hines, K. E., J. R. Bankston, and R. W. Aldrich (2015). Analyzing single-molecule time series via nonparametric bayesian inference. *Biophysical Journal 108*(3), 540 – 556.

[40] Hituri, K. and M.-L. Linne (2013). Comparison of models for IP_3 receptor kinetics using stochastic simulations. *PLoS ONE 8*(4), e59618.

[41] Hodgson, M. E. A. and P. J. Green (1999, SEP 8). Bayesian choice among Markov models of ion channels using Markov chain Monte Carlo. *Proceedings of the Royal Society of London Series A-Mathematical Physical and Engineering Sciences 455*(1989), 3425–3448.

[42] Höfer, T., L. Venance, and C. Giaume (2002). Control and plasticity of intercellular calcium waves in astrocytes: A modeling approach. *The Journal of Neuroscience 22*(12), 4850–4859.

[43] Holtzclaw, L., S. Pandhit, D. Bare, G. Mignery, and J. Russell (2002). Astrocytes in adult rat brain express type 2 inositol 1,4,5-trisphosphate receptors. *GLIA 39*(1), 69–84. cited By 0.

[44] Ionescu, L., C. White, K.-H. Cheung, J. Shuai, I. Parker, J. E. Pearson, J. K. Foskett, and D.-O. D. Mak (2007). Mode switching is the major mechanism of ligand regulation of $InsP_3$ receptor calcium release channels. *Journal of General Physiology 130*(6), 631–645.

[45] Lallouette, J., M. De Pittà, E. Ben-Jacob, and H. Berry (2014). Sparse short-distance connections enhance calcium wave propagation in a 3d model of astrocyte networks. *Frontiers in Computational Neuroscience 8*(1 APR), 45. cited By 2.

[46] Lavrentovich, M. and S. Hemkin (2008). A mathematical model of spontaneous calcium(ii) oscillations in astrocytes. *Journal of Theoretical Biology 251*(4), 553–560. cited By 18.

[47] Li, B., S. Chen, S. Zeng, Q. Luo, and P. Li (2012). Modeling the contributions of Ca^{2+} flows to spontaneous Ca^{2+} oscillations and cortical spreading depression-triggered Ca^{2+} waves in astrocyte networks. *PLoS ONE 7*(10), e48534. cited By 1.

[48] Li, Y.-X. and J. Rinzel (1994). Equations for InsP3 receptor-mediated $[Ca^{2+}]_i$ oscillations derived from a detailed kinetic model: A Hodgkin-Huxley like formalism. *Journal of Theoretical Biology 166*(4), 461 – 473.

[49] Ludtke, S. J. and I. I. Serysheva (2013). Single-particle cryo-EM of calcium release channels: structural validation. *Current Opinion in Structural Biology 23*, 755–762.

[50] Macdonald, C. and G. Silva (2013). A positive feedback cell signaling nucleation model of astrocyte dynamics. *Frontiers in Neuroengineering 6*, 4. cited By 0.

[51] Magleby, K. L. and B. S. Pallotta (1983a). Burst kinetics of single calcium-activated potassium channels in cultured rat muscle. *Journal of Physiology-London 344*, 605–623.

[52] Magleby, K. L. and B. S. Pallotta (1983b). Calcium dependence of open and shut interval distributions from calcium-activated potassium channels in cultured rat muscle. *Journal of Physiology-London 344*, 585–604.

[53] Mak, D.-O. D. and J. K. Foskett (2015). Inositol 1,4,5-trisphosphate receptors in the endoplasmic reticulum: A single-channel point of view. *Cell Calcium 58*(1), 67 – 78. SI: Organellar Channels & Transporters.

[54] Mak, D.-O. D., J. E. Pearson, K. P. C. Loong, S. Datta, M. Fernández-Mongil, and J. K. Foskett (2007). Rapid ligand-regulated gating kinetics of single inositol 1,4,5-trisphosphate receptor ca^{2+} release channels. *EMBO reports 8*(11), 1044–1051.

[55] Marchant, J., N. Callamaras, and I. Parker (1999). Initiation of IP_3-mediated Ca^{2+} waves in xenopus oocytes. *EMBO Journal 18*, 5285–5299.

[56] Neher, E. and B. Sakmann (1976). Single-channel currents recorded from membrane of denervated frog muscle fibres. *Nature 260*(5554), 799–802.

[57] Parker, I., J. Choi, and Y. Yao (1996). Elementary events of $InsP_3$-induced Ca^{2+} liberation in *xenopus* oocytes: hot spots, puffs and blips. *Cell Calcium 20*(2), 105 – 121.

[58] Parys, J. B., S. W. Sernett, S. DeLisle, P. M. Snyder, M. J. Welsh, and K. P. Campbell (1992). Isolation, characterization, and localization of the inositol 1,4,5-trisphosphate receptor protein in Xenopus laevis oocytes. *The Journal of Biological Chemistry 267*(26), 18776–18782.

[59] Postnov, D., R. Koreshkov, N. Brazhe, A. Brazhe, and O. Sosnovtseva (2009). Dynamical patterns of calcium signaling in a functional model of neuron-astrocyte networks. *Journal of Biological Physics 35*(4), 425–445. cited By 0.

[60] Qin, F., A. Auerbach, and F. Sachs (1996). Idealization of single-channel currents using the segmental K-means method. *Biophysical Journal 70*(2, Part 2), MP432.

[61] Qin, F., A. Auerbach, and F. Sachs (1997). Maximum likelihood estimation of aggregated Markov processes. *Proceedings of the Royal Society of London Series B-Biological Sciences 264*, 375–383.

[62] Riera, J., R. Hatanaka, T. Ozaki, and R. Kawashima (2011). Modeling the spontaneous Ca^{2+} oscillations in astrocytes: Inconsistencies and usefulness. *Journal of Integrative Neuroscience 10*(04), 439–473. PMID: 22262535.

[63] Riera, J., R. Hatanaka, T. Uchida, T. Ozaki, and R. Kawashima (2011). Quantifying the uncertainty of spontaneous Ca^{2+} oscillations in astrocytes: Particulars of Alzheimer's disease. *Biophysical Journal 101*(3), 554–564. cited By 6.

[64] Rosales, R. (2004). MCMC for Hidden Markov Models incorporating aggregation of states and filtering. *Bulletin of Mathematical Biology 66*, 1173–1199.

[65] Rosales, R., J. A. Stark, W. J. Fitzgerald, and S. B. Hladky (2001). Bayesian Restoration of Ion Channel Records using Hidden Markov Models. *Biophysical Journal 80*(3), 1088–1103.

[66] Rüdiger, S. (2014). Stochastic models of intracellular calcium signals. *Physics Reports 534*(2), 39 – 87. Stochastic models of intracellular calcium signals.

[67] Rüdiger, S., J. Shuai, W. Huisinga, C. Nagaiah, G. Warnecke, I. Parker, and M. Falcke (2007). Hybrid stochastic and deterministic simulations of calcium blips. *Biophysical Journal 93*(6), 1847 – 1857.

[68] Seneta, E. (1981). *Non-negative Matrices and Markov Chains* (2 ed.). Springer Series in Statistics. New York: Springer.

[69] Sharp, A. H., F. C. Nucifora Jr., O. Blondel, C. A. Sheppard, C. Zhang, S. H. Snyder, J. T. Russell, D. K. Ryugo, and C. A. Ross (1999). Differential cellular expression of isoforms of inositol 1,4,5-triphosphate receptors in neurons and glia in brain. *Journal of Comparative Neurology 406*(2), 207–220. cited By 0.

[70] Siekmann, I., E. J. Crampin, and J. Sneyd (2012). MCMC can detect non-identifiable models. *Biophysical Journal 103*(11), 1275–1286.

[71] Siekmann, I., M. Fackrell, E. J. Crampin, and P. Taylor (2016). Modelling modal gating of ion channels with hierarchical markov models. *Proceedings of the Royal Society of London A 472*, 20160122.

[72] Siekmann, I., J. Sneyd, and E. J. Crampin (2014, June). Statistical analysis of modal gating in ion channels. *Proceedings of the Royal Society of London A 470*(2166), 20140030.

[73] Siekmann, I., L. E. Wagner II, D. Yule, E. J. Crampin, and J. Sneyd (2012). A kinetic model of type I and type II IP_3R accounting for mode changes. *Biophysical Journal 103*(4), 658–668.

[74] Siekmann, I., L. E. Wagner II, D. Yule, C. Fox, D. Bryant, E. J. Crampin, and J. Sneyd (2011). MCMC estimation of Markov models for ion channels. *Biophysical Journal 100*, 1919–1929.

[75] Smith, I. F. and I. Parker (2009). Imaging the quantal substructure of single IP_3R channel activity during Ca^{2+} puffs in intact mammalian cells. *Proceedings of the National Academy of Sciences of the USA 106*(15), 6404–6409.

[76] Sneyd, J., A. Charles, and M. Sanderson (1994). A model for the propagation of intercellular calcium waves. *American Journal of Physiology - Cell Physiology 266*(1 35-1), C293–C302. cited By 51.

[77] Sneyd, J. and M. Falcke (2005). Models of the inositol trisphosphate receptor. *Progress in Biophysics and Molecular Biology 89*, 207–245.

[78] Sneyd, J., M. Falcke, J. F. Dufour, and C. Fox (2004). A comparison of three models of the inositol trisphosphate receptor. *Progress in Biophysics and Molecular Biology 85*, 121–140.

[79] Swillens, S., L. Combettes, and P. Champeil (1994). Transient inositol 1,4,5-trisphosphate-induced Ca^{2+} release: a model based on regulatory Ca(2+)-binding sites along the permeation pathway. *Proceedings of the National Academy of Sciences 91*(21), 10074–10078.

[80] Thurley, K., A. Skupin, R. Thul, and M. Falcke (2012). Fundamental properties of Ca^{2+} signals. *Biochimica et Biophysica Acta 1820*(8), 1185–1194.

[81] Thurley, K., I. F. Smith, S. C. Tovey, C. W. Taylor, I. Parker, and M. Falcke (2011). Timescales of IP_3-evoked Ca^{2+} spikes emerge from Ca^{2+} puffs only at the cellular level. *Biophysical Journal 101*, 2638–2644.

[82] Tu, H., Z. Wang, and I. Bezprozvanny (2005). Modulation of mammalian inositol 1,4,5-trisphosphate receptor isoforms by calcium: A role of calcium sensor region. *Biophysical Journal 88*(2), 1056–1069. cited By 57.

[83] Ullah, G., W. J. Bruno, and J. E. Pearson (2012). Simplification of reversible Markov chains by removal of states with low equilibrium occupancy. *Journal of Theoretical Biology 311*(0), 117–129.

[84] Ullah, G., D.-O. D. Mak, and J. E. Pearson (2012). A data-driven model of a modal gated ion channel: The inositol 1,4,5-trisphosphate receptor in insect Sf9 cells. *Journal of General Physiology 140*(2), 159–173.

[85] Ullah, G., I. Parker, D. O. D. Mak, and J. E. Pearson (2012). Multi-scale data-driven modeling and observation of calcium puffs. *Cell Calcium 52*, 152–160.

[86] Wagner, L. E. and D. I. Yule (2012). Differential regulation of the $InsP_3$ receptor type-1 and -2 single channel properties by $InsP_3$, Ca^{2+} and ATP. *The Journal of Physiology 590*(14), 3245–3259.

[87] Zeng, S., B. Li, S. Zeng, and S. Chen (2009). Simulation of spontaneous Ca^{2+} oscillations in astrocytes mediated by voltage-gated calcium channels. *Biophysical Journal 97*(9), 2429–2437. cited By 9.